Comparative study of rutile and anatase SnO2 and TiO2: Band-edge structures, dielectric functions, and polaron effects

Maofeng Dou and Clas Persson

Articles you may be interested in

Optical properties of amorphous and crystalline Sb-doped SnO2 thin films studied with spectroscopic ellipsometry: Optical gap energy and effective mass
J. Appl. Phys. **118**, 085303 (2015); 10.1063/1.4929487

Ordinary and extraordinary dielectric functions of rutile SnO2 up to 20 eV
Appl. Phys. Lett. **104**, 231106 (2014); 10.1063/1.4882237

Contrasting the experimental properties of hydrogen in SnO2, In2O3, and TiO2
J. Appl. Phys. **115**, 012001 (2014); 10.1063/1.4837955

Strong polaronic effects on rutile TiO 2 electronic band edges
Appl. Phys. Lett. **86**, 231912 (2005); 10.1063/1.1940739

Comparison of thin film and bulk forms of the transparent conducting oxide solution Cd 1+x In 2−2x Sn x O 4
J. Appl. Phys. **90**, 5979 (2001); 10.1063/1.1410882

CrossMark
click for updates

Comparative study of rutile and anatase SnO₂ and TiO₂: Band-edge structures, dielectric functions, and polaron effects

Maofeng Dou[1,a)] and Clas Persson[1,2]

[1]*Department of Materials Science and Engineering, Royal Institute of Technology, SE-100 44 Stockholm, Sweden*
[2]*Department of Physics, University of Oslo, P. O. Box 1048 Blindern, NO-0316 Oslo, Norway*

SnO₂ and TiO₂ polymorphs (rutile and anatase) are oxides with similar crystal structures, comparable bond lengths, and electronic band-gap energies, but different optical and electronic properties. In this work, we have studied the origin of these differences from the band-edge structures and electron-phonon coupling. The band-edge structures, dielectric functions, and effective masses were calculated by means of a first-principles approach with the exchange-correlation described by a hybrid functional. The phonon frequencies were calculated using a finite displacement method with non-analytic correction, and the phonon contribution to the dielectric functions was modeled using a multi-phonon Lorentz model. The calculated band-edge structures show that the bottommost conduction bands are highly dispersive for SnO₂ polymorphs but flat dispersive for TiO₂ polymorphs because of the strongly localized Ti-3d states. Consequently, SnO₂ polymorphs present small effective electron masses and a weak optical absorption, whereas the TiO₂ polymorphs present a strong optical absorption and larger effective electron masses. Due to the strong ionic bonds, TiO₂ have larger Born effective charges than that of SnO₂, result in stronger polaron effect and larger average static dielectric constant ε^0. For example, $\varepsilon^0 = 115$ for rutile TiO₂ whereas $\varepsilon^0 = 9.5$ for rutile SnO₂. Moreover, it is interesting to note that the ε^0 in rutile TiO₂ is much larger than in anatase TiO₂ ($\varepsilon^0 = 28$) although they have the same chemical compositions, which related to the local structure distortion of the phases. © *2013 American Institute of Physics.*
[http://dx.doi.org/10.1063/1.4793273]

I. INTRODUCTION

SnO₂ and TiO₂ are important oxides in (opto)electronic technologies involving efficient dielectrics, catalysis, sensors, thin-film transistors, and other transparent electronic devices.[1–3] Both SnO₂ and TiO₂ can be grown in the rutile crystalline structure (space group no. 136; D_{4h}^{14}; $P4_2/mnm$), and TiO₂ can also be formed in the anatase phase (no. 141; D_{4h}^{19}; $I4_1/amd$); see Fig. 1. Although SnO₂ and TiO₂ have similar crystal structures, comparable bond lengths (∼1.90 Å), similar chemical bonds, and comparable electronic band-gap energies ($E_g \approx$ 3–4 eV), the optical and electronic properties however are quite different, e.g., SnO₂ is typically optical transparent with large electron conductivity; TiO₂ is optical absorption favorable with weak electrons mobility due to electrons and holes trapping. These quantities are primarily determined by the details in the energy dispersion $E_n(\mathbf{k})$ of the band edges and the phonon-electron coupling. SnO₂ and TiO₂ have been studied for many years, but basic calculations can be still valuable to provide the fundamental data for devices simulation, e.g., oxide thin-film transistor, dye-sensitive solar cell. Moreover, a comparative study of the band-edge structures and polaron effect would also help to understand the origin of these differences and provide a guideline for further design the materials to improve related properties, e.g., charges mobility, separation, and detrapping.

We have previously presented the optical properties[4] of F-doped rutile SnO₂ (r-SnO₂), the polaron effect[5] in rutile TiO₂ (r-TiO₂), and the band-edges absorption[6] of r-SnO₂ and r-TiO₂. Those calculations were based on the local density approximation (LDA) in combination with on-site Coulomb potential (LDA + U^{SIC}) approach[7] to describe the cation-d electrons.

In this work, we analyze the band-edge structures, the dielectric functions, and the polaron effect of SnO₂ and TiO₂ rutile and anatase polymorphs (the anatase compounds are denoted as a-SnO₂ and a-TiO₂). The Heyd-Scuseria-Ernzerhof (HSE)[8] hybrid functional, in which the Hartree-Fock functional mixed with generalized gradient approximation (GGA) functional, was used to calculate the band-edges structures and the dielectric function. Since these calculations neglected the electron-phonon coupling, the phonon part dielectric functions together with the polaron effect were modeled with classic models.

II. COMPUTATIONAL DETAILS

The electronic structures calculations were performed based on projector augmented wave (PAW)[9] method and plane-wave basis set with cutoff energy of 400 eV. The exchange-correlation potential was described by the HSE functional in which the short-range exchange potential is combination of 25% Hartree-Fock exchange potential with

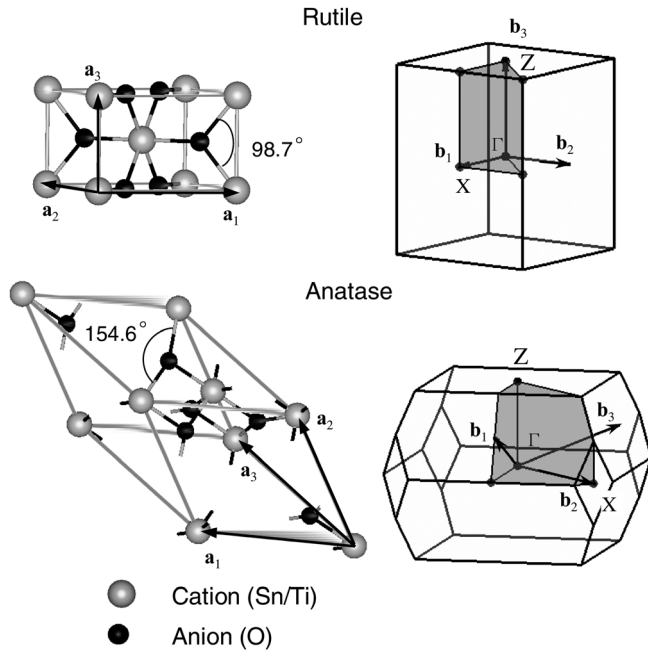a)Author to whom correspondence should be addressed. Electronic mail: Maofeng.Dou@mse.kth.se.

Rutile

Anatase

○ Cation (Sn/Ti)

● Anion (O)

FIG. 1. The crystalline structures and Brillouin zones of rutile D_{4h}^{14} and anatase D_{4h}^{19}. The crystal structures are optimized via the HSE approach with: $a = 4.737$ Å; $c = 3.186$ Å for rutile SnO$_2$ (r-SnO$_2$), $a = 4.592$ Å; $c = 2.948$ Å for rutile TiO$_2$ (r-TiO$_2$), $a = 3.975$ Å; $c = 10.203$ Å for anatase SnO$_2$ (a-SnO$_2$), and $a = 3.766$ Å; $c = 9.636$ Å for anatase TiO$_2$ (a-TiO$_2$). The optimization reveals that and internal lattice parameter u is fairly similar for SnO$_2$ and TiO$_2$: $u = 0.306$ for r-SnO$_2$ and 0.305 for r-TiO$_2$, whereas $u = 0.800$ for a-SnO$_2$ and 0.794 for a-TiO$_2$.

75% Perdew-Burke-Ernzerhof (PBE) potential with the screening parameter of 0.2 Å^{-1}. The band-gap energy was also predicted using partly self-consistent single-particle Green's function (GW$_0$) approach in which the internal cut-off energy was set to 100 eV. The Brillouin-zone integration was performed with a Γ-centered symmetry reduced automatically an $8 \times 8 \times 8$ k-mesh in the first Brillouin zone for HSE and a $6 \times 6 \times 6$ k-mesh for the GW$_0$ calculation.

Phonon frequencies were calculated based on $2 \times 2 \times 2$ supercells by means of the finite displacement approach.[10] The longitudinal-transverse optical (LO-TO) phonon splitting in the vicinity of the Γ-point was corrected using a non-analytical correction.[11] The Born effective charges Z*, which are essential for calculating the non-analytical term, were calculated with the homogenous electrical field method.

The dielectric functions excluding the phonon contributions were determined from the joint density-of-states (DOS) and the optical momentum matrix in the long wave length $q = |\mathbf{k}' - \mathbf{k}| = 0$ limit[12]

$$\varepsilon_{2,\alpha\beta}(\omega) = \frac{4\pi e^2}{\Omega} \lim_{q \to 0} \frac{1}{q} \sum_{c,v,\mathbf{k}} 2w_{\mathbf{k}}\delta(E_{c\mathbf{k}} - E_{v\mathbf{k}} - \hbar\omega)$$
$$\times \langle u_{c\mathbf{k}+\mathbf{e}_\alpha q}|u_{v\mathbf{k}}\rangle\langle u_{c\mathbf{k}+\mathbf{e}_\beta q}|u_{v\mathbf{k}}\rangle, \quad (1)$$

where e is the electron charge, Ω is the primitive cell volume, $w_{\mathbf{k}}$ is the weight of $\mathbf{k}$-points; v and c present the valence and conduction bands, respectively, α and β present the
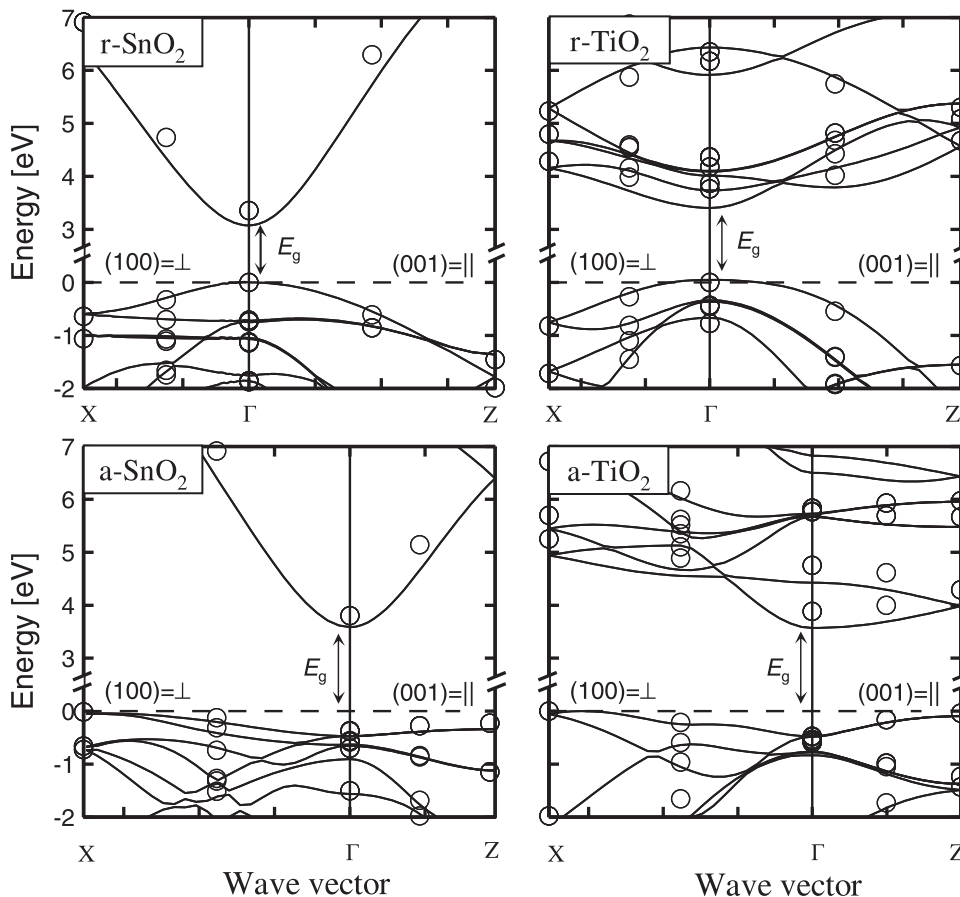

FIG. 2. Electronic structures of r-SnO$_2$, r-TiO$_2$, a-SnO$_2$, and a-TiO$_2$ along two main symmetry directions $(100) = \perp$ and $(001) = \parallel$. Solid lines and circles represent the HSE and GW$_0$ energies, respectively. Energies refer to the VBM. Spin-orbit interaction is included.

Cartesian directions, $\mathbf{e}_\alpha$ and $\mathbf{e}_\beta$ are unit vectors for the three Cartesian directions; $u_{v\mathbf{k}}$ is the periodic part of Bloch wave function corresponding to the eigenvalue $E_{c\mathbf{k}}$. The Dirac-delta function indicates the importance of describing the band gap correctly. The real part of the dielectric function is obtained from the Kramers-Kronig transformation.

The phonon parts of the dielectric functions were modeled using the Lorentz model and the Kramers-Heisenberg formula with multi-phonon contributions[13]

$$\varepsilon_{phonon}(\omega) = \sum_j \varepsilon_j^\infty \cdot \frac{\omega_{LO,j}^2 - \omega_{TO,j}^2}{\omega_{TO,j}^2 - \omega^2 - i\gamma_j\omega}, \qquad (2)$$

where $\omega_{TO,j}$ and $\omega_{LO,j}$ are the LO and TO phonon frequency of jth phonon mode, ε_j^∞ is the high frequency dielectric constant of the jth phonon mode, and γ_j is the damping parameter which was set to $\gamma_j \to 0$.

III. RESULTS

A. Band-edge structures

The band structures of SnO$_2$ and TiO$_2$ along the $\Gamma-X$ (100) and $\Gamma-Z$ (001) directions are presented in Fig. 2. The electronic energies were calculated with both the HSE and GW$_0$ approaches, and the relevant Γ-point values are listed in Table I together with the experimental values. The rutile structures have direct band gap with both the valence-band maximum (VBM) and conduction-band minimum (CBM) at the Γ-point. For r-SnO$_2$, both calculation approaches fairly, accurately estimate the band-gap energy (3.07 eV with HSE and 3.36 eV with GW$_0$) compared to the experimental data (3.3–4.0 eV).[14] For r-TiO$_2$, however, the band-gap energy was accurately calculated by HSE (3.36 eV) but slightly overestimated by GW$_0$ (3.77 eV) compared to the experimental data (3.3–3.3 eV).[15,16] It has been demonstrated that the GW$_0$ band gap of TiO$_2$ varies with the approximation methods on the self-energy. The changes in the correlation part of the self-energy of the CBs orbitals are sensitive to the GW methods.[16] The anatase structure has indirect band gap with CBM at the Γ-point and VBM along the (100) direction. Similar to the case of rutile structure, the band gap of a-TiO$_2$ calculated with HSE (3.57 eV) agrees well with experimental values (3.2–3.4 eV)[17,18] but was overestimated by the GW$_0$ approach (3.89 eV). Although the band-gap energies of SnO$_2$ and TiO$_2$ are comparable, the band-edge structures, which are essentially determined by the crystal symmetry and chemical composition, are different. The VBs of both r-SnO$_2$ and r-TiO$_2$ are flat dispersed in both the longitudinal (∥) and transverse (⊥) directions with the Γ_7^+ symmetry at VBM. The CBs, however, are quite different. r-SnO$_2$ has single, highly dispersive band at CBs (the energy difference between c$_1$ and c$_2$ is 5.1 eV at Γ point; with c$_1$ and c$_2$ refers to the bottommost and second CB, respectively) whereas r-TiO$_2$ has several energetically close-lying and flat dispersed CBs (the energy differences between c$_1$ and c$_2$ is only 0.3; see Figs. 2 and 3). Similar with the case of rutile, the VBs of both a-SnO$_2$ and a-TiO$_2$ are also flat dispersed in both ∥ and ⊥ directions. The a-SnO$_2$ has single and highly dispersive CBs (the energy difference between c$_1$ and c$_2$ is 4.3 eV),

TABLE I. Calculated Γ-point band energies $E_n(\Gamma)$ of rutile SnO$_2$(r-SnO$_2$), rutile TiO$_2$(r-TiO$_2$), anatase SnO$_2$(a-SnO$_2$), and anatase TiO$_2$(a-TiO$_2$) in units of eV and referred to the VBM; cf. Figs. 2 and 3. Spin-orbit coupling is included. The c$_1$ refers to the bottommost of CB, v$_1$, v$_2$, and v$_3$ refer to the uppermost, second, and third VB, respectively; see Fig. 3.

	HSE	GW$_0$	Expt.
r-SnO$_2$			
$E_{c2}(\Gamma_7^+)$	8.14	8.29	
$E_{c1}(\Gamma_6^+)$	3.07	3.35	3.3–4.0[a]
$E_{v1}(\Gamma_7^+)$	0.00	0.00	
$E_{v2}(\Gamma_7^-)$	−0.72	−0.72	
$E_{v3}(\Gamma_6^-)$	−0.75	−0.74	
r-TiO$_2$			
$E_{c2}(\Gamma_7^+)$	3.74	4.00	
$E_{c1}(\Gamma_6^+)$	3.36	3.77	3.1,[b] 3.3[c]
$E_{v1}(\Gamma_7^+)$	0.00	0.00	
$E_{v2}(\Gamma_7^-)$	−0.38	−0.43	
$E_{v3}(\Gamma_6^-)$	−0.41	−0.45	
a-SnO$_2$			
$E_{c2}(\Gamma_7^-)$	7.86	8.88	
$E_{c1}(\Gamma_6^+)$	3.58	3.80	
$E_{v1}(\Gamma_6^+)$	−0.47	−0.37	
$E_{v2}(\Gamma_7^+)$	−0.48	−0.38	
$E_{v3}(\Gamma_7^-)$	−0.63	−0.56	
a-TiO$_2$			
$E_{c2}(\Gamma_7^+)$	4.43	4.75	
$E_{c1}(\Gamma_6^-)$	3.57	3.89	3.2,[d] 3.4[e]
$E_{v1}(\Gamma_6^+)$	−0.48	−0.47	
$E_{v2}(\Gamma_7^+)$	−0.49	−0.48	
$E_{v3}(\Gamma_7^-)$	−0.77	−0.53	

[a]Reference 14.
[b]Reference 15.
[c]Reference 16.
[d]Reference 17.
[e]Reference 18.

whereas a-TiO$_2$ has several energetically close-lying and flat dispersed CBs (the energy difference between c$_1$ and c$_2$ is 0.8 eV). This difference is a consequence of the different cation valence electron configurations, i.e., $5s^25p^2$ for Sn and $3d^24s^2$ for Ti. The delocalized Sn-5s states dominate the CBs in SnO$_2$ polymorphs giving rise to high dispersive CBs, whereas the strongly localized Ti-3d states dominate the CBs in TiO$_2$ polymorphs giving rise to the flat CBs (Fig. 4). All four compounds have flat dispersed VBs in both the ∥ and the ⊥ directions because of the same anion valence electron configurations, i.e., O-2$s^2$2p^2, which dominates the upper VBs. The spin-orbit coupling has strong effect on the second and third VBs for r-SnO$_2$ and r-TiO$_2$ with the energy split $\Delta_{so} = 30$ and 27 meV, respectively. For a-SnO$_2$ and a-TiO$_2$, the energy split is $\Delta_{so} = 40$ and 11 meV, respectively.

In Table II, we present the calculated effective bare electron ($m_{c_1}^*$) and hole ($m_{v_1}^*$) masses obtained from a parabolic fitting of the band dispersive around the VBM and CBM. Available experimental values are also presented for comparison.[19–21] In the rutile structure, both SnO$_2$ and TiO$_2$ have large effective hole masses ($m_{v_1,\perp}^* = 1.27$ and $m_{v_1,\parallel}^* = 1.60$ for r-SnO$_2$; $m_{v_1,\perp}^* = 2.79$ and $m_{v_1,\parallel}^* = 3.77$
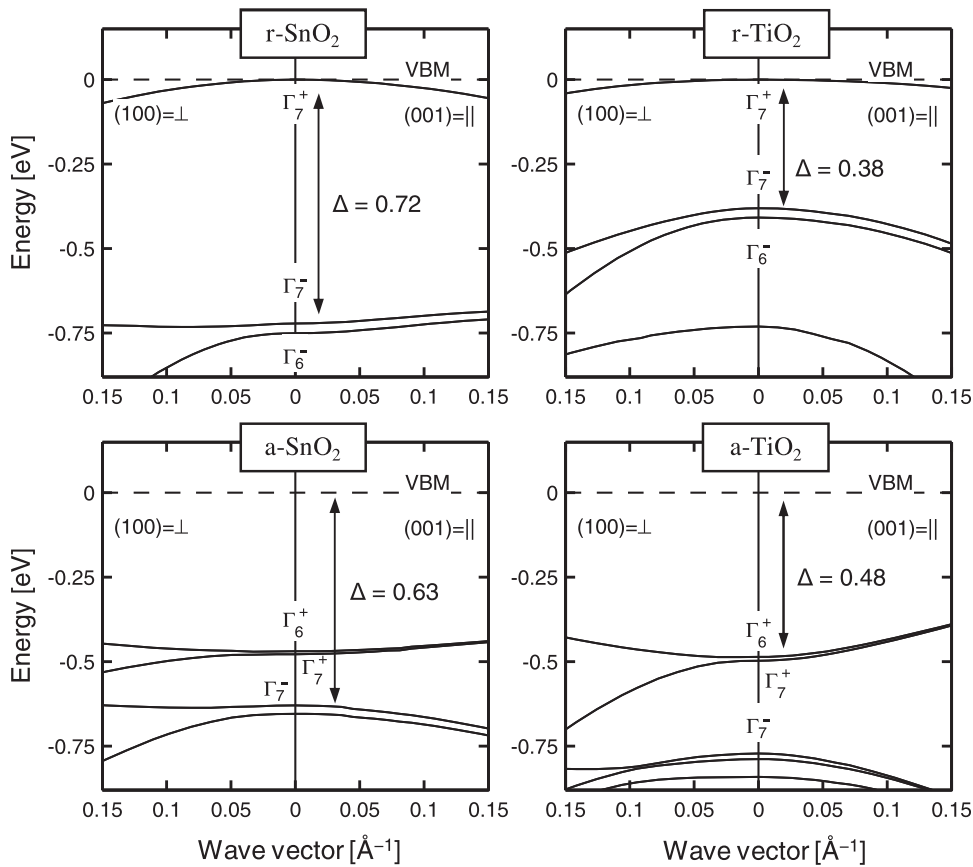
FIG. 3. Close-up of the topmost VBs at the VBM from Fig. 2.

for r-TiO$_2$) which is due to the flat dispersion of the first VB as discussed above. The effective electron masses in r-TiO$_2$ are much larger than in r-SnO$_2$ ($m^*_{c_1,\perp} = 1.11$ and $m^*_{c_1,\parallel} = 0.57$ for r-TiO$_2$ whereas $m^*_{c_1,\perp} = 0.25$ and $m^*_{c_1,\parallel} = 0.21$ for r-SnO$_2$). This is a consequence of the strong localized d states which also contribute to the strong anisotropy of effective electron mass in r-TiO$_2$ (i.e., $m^*_{c_1,\perp}/m^*_{c_1,\parallel} = 1.95$ for r-TiO$_2$ whereas $m^*_{c_1,\perp}/m^*_{c_1,\parallel} = 1.19$ for r-SnO$_2$). For anatase, the effective masses follow the same trend as for rutile phase: a-TiO$_2$ has larger anisotropic effective electron masses ($m^*_{c_1,\perp} = 0.26$ and $m^*_{c_1,\parallel} = 0.24$; $m^*_{c_1,\perp}/m^*_{c_1,\parallel} = 0.13$).

B. Dielectric function

The dielectric function $\varepsilon(\omega) = \varepsilon_1(\omega) + i\varepsilon_2(\omega)$ describes the electronic response to a small change in the charge distribution. This response is an important property for describing electronic screening near dopants, defects, dislocations, and other structural perturbations. The imaginary $\varepsilon_2(\omega)$ and real $\varepsilon_1(\omega)$ parts of the dielectric functions of SnO$_2$ and TiO$_2$ are shown in Figs. 5 and 6. For all four compounds, the direct optical onset does not occur at photon energies $\hbar\omega \approx E_g$ as one may expect. Instead, the onset is above the band-gap energies, at the energy $E_g + \Delta$. The optical onset occurs at $E_g + \Delta \approx 3.79$ eV for r-SnO$_2$ and $E_g + \Delta \approx 3.74$ eV for r-TiO$_2$ corresponding to the transitions form second VB (Γ_7^-) to CBM (Γ_6^+) at Γ point. The transitions between the VBM (Γ_7^+) and CBM (Γ_6^+) are symmetry forbidden for both the

longitudinal and transverse polarizations. Although transitions are symmetry allowed[5,22] away from the Γ point, the smooth changed orbitals, i.e., s- and p-like orbitals, at the uppermost VB present low transitions rate which may explain the measured weak near band-gap optical absorption.[23] The measured larger optical peaks[23] of r-TiO$_2$ in the energy range of 4.0 to 6.0 eV can be understood from the band-edges structures: the bands involving the direct transition in r-TiO$_2$ near $E_g + \Delta$ are more than r-SnO$_2$ due to the energetically close-lying CBs in r-TiO$_2$. This originates from different properties of the SnO$_2$ and TiO$_2$ electronic structures. The rutile phases have direct Γ-point band-gap, whereas the anatase compounds have indirect band gap. This explains the onset $E_g + \Delta$ in a-SnO$_2$ and a-TiO$_2$. Moreover, the dipole induced optical transition is restricted not only by the energy conservations but also by the selection rules of the transition. In rutile structure, the transitions between the uppermost VB and the bottommost CB are forbidden due to the symmetry of the VB and CB wavefunctions. This explains the high onset energy for absorption in r-SnO$_2$ and r-TiO$_2$. The overall shapes of the dielectric functions of both r-SnO$_2$ and r-TiO$_2$ are comparable with the experimental measurements[24] except for large excitons absorption which is excluded in our dielectric function calculations. The polarons can further change the dielectric functions especially for r-TiO$_2$ which has large ionic screening. Concerning the anatase structure, the calculated optical transitions on-set of the transverse polarization occur at $E_g + \Delta \approx 4.21$ eV for a-SnO$_2$ but below the $E_g + \Delta$ for a-TiO$_2$ (at $\sim$3.9 eV) which is
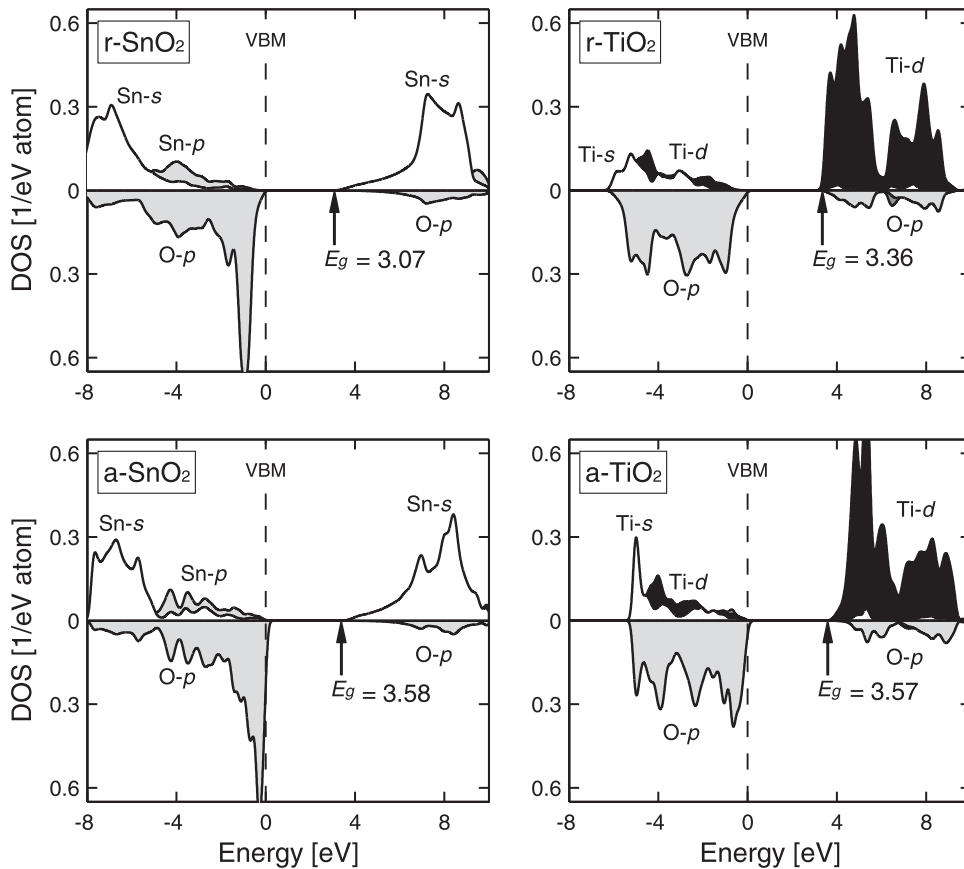
FIG. 4. Atom and angular resolved DOS near the band-edges of r-SnO$_2$, r-TiO$_2$, a-SnO$_2$, and a-TiO$_2$, using the HSE functional and including a 0.03 eV Lorentzian broadening. The DOS has been scaled by $(2l+1)^{-1}$ for better visibility. The main difference between SnO$_2$ and TiO$_2$ is the strong cation $3d$-character of the lowest CBs of TiO$_2$.

comparable with the a-TiO$_2$ optical absorption measurement.[24] In a-TiO$_2$, the energy difference between the uppermost VB and bottommost CB along the $\Gamma-Z$ direction is smaller than $E_g + \Delta$ at Γ point due to the flat band dispersion of the uppermost VB along the $\Gamma-Z$ direction. The optical absorption on-set thus is below $E_g + \Delta$ for transverse

polarization transitions involving the **k** points along $\Gamma-Z$ direction.[25] Similar with r-TiO$_2$, the experimentally observed weak absorptions below the direct transition in a-TiO$_2$ does not occur in the calculated $\varepsilon_2(\omega)$ due to the excluding phonon and exciton effect. The calculated high-frequency dielectric constants (Table III) for both SnO$_2$ and TiO$_2$ polymorphs are

TABLE II. The calculated effective electron and hole masses m_c^* and m_v^* at CBM and VBM together with the available experimental values. The corresponding polaron masses m^p are also listed. The spin-orbit coupling is included.

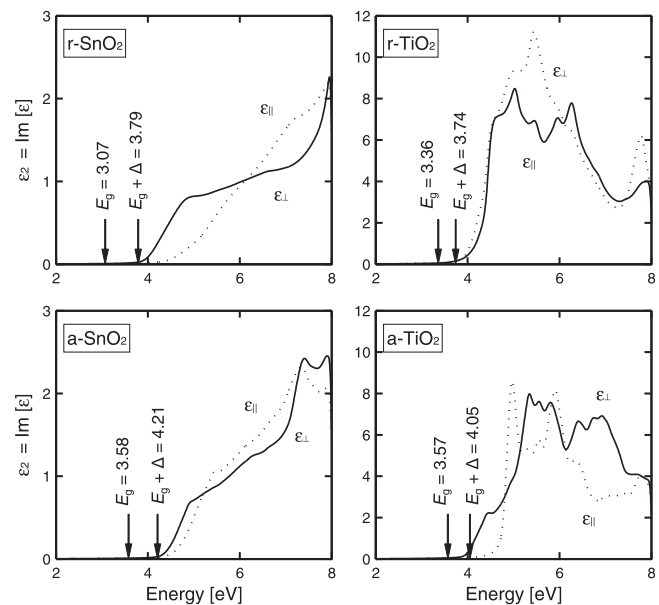|	$m^*(m_0)$		$m^p(m_0)$		Expt.
	$(100)=\perp$	$(001)=\parallel$	$(100)=\perp$	$(001)=\parallel$	
r-SnO$_2$					
c_1 (Γ_6^+)	0.25	0.21	0.46	0.26	0.41[a]
v_1 (Γ_7^+)	1.27	1.60	3.62	2.74	
r-TiO$_2$					
c_1 (Γ_6^+)	1.11	0.57	2.43	0.899	20[b]
v_1 (Γ_7^+)	2.79	3.77	8.05	9.36	
a-SnO$_2$					
c_1 (Γ_6^+)	0.26	0.24	0.33	0.29	
v_1	1.15	1.23	1.83	1.59	
a-TiO$_2$					
c_1 (Γ_6^-)	0.42	3.36	0.75	7.28	
v_1	1.62	0.93	4.12	1.50	1.0[c]

[a]Reference 19.
[b]Reference 20.
[c]Reference 21.

FIG. 5. The imaginary part $\varepsilon_2(\omega)$ of the dielectric function from the HSE calculations of r-SnO$_2$, r-TiO$_2$, a-SnO$_2$, and a-TiO$_2$. The spectra are divided into transverse ($\perp$) and longitudinal ($\parallel$) components, including a 0.03 eV Lorentzian broadening.
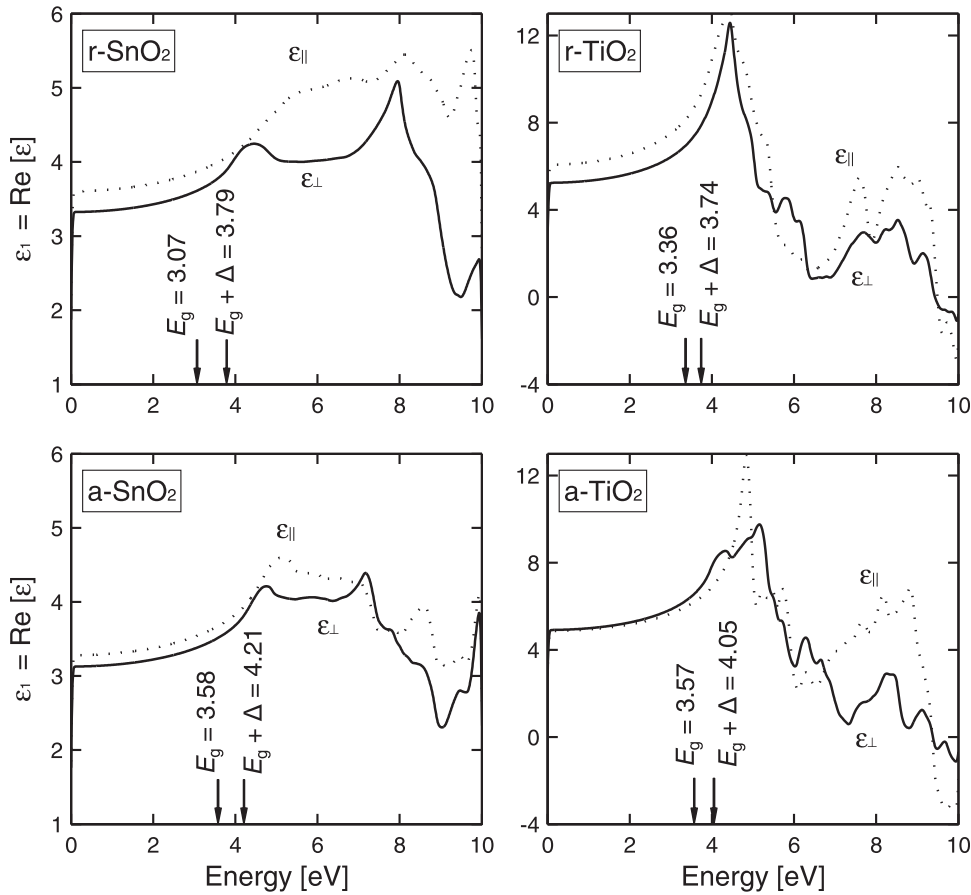
FIG. 6. The real part $\varepsilon_1(\omega)$ of the dielectric function obtained from the Kramers-Kronig transformation.

anisotropy which agree very well with experimental results.[26–29] Overall, the calculated dielectric functions indicate that the TiO$_2$ polymorphs favor a stronger optical absorption than the SnO$_2$ polymorphs due to the energetically close-lying and flat dispersed bands near the band-edge.

C. Phonon frequencies

In both SnO$_2$ and TiO$_2$, there are 15 optical modes and 3 acoustic modes. The irreducible representations corresponding to the 15 optical modes are A$_{1g}$ + A$_{2g}$ + A$_{2u}$ + B$_{1g}$ +

2B$_{1u}$ + B$_{2g}$ + E$_g$ + 3E$_u$ for rutile[30] and A$_{1g}$ + A$_{2u}$ + 2B$_{1g}$ + B$_{1u}$ + 3E$_g$ + 2E$_u$ for anatase.[31] The infrared active modes E$_u$ and A$_{2u}$ are the most important for studying the lattice response in the presence of an external field. In the rutile structure, there are three degenerated E$_u$ modes and one A$_{2u}$ mode corresponding to the displacement of the cation and anion, respectively, along the [110] and [001] directions. This generates a LO-TO splitting when the phonon wave vector approaching the Γ-point in the direction parallel to the displacements. In the anatase structure, there are two E$_u$ modes and one A$_{2u}$ mode corresponding to the displacement along the [100] and [001] directions, respectively. The calculated phonon frequencies in the vicinity of the Γ point are listed in Table IV together with the measurement data.[29,30,32,33] We use $[(\omega_{LO,j}^2 - \omega_{TO,j}^2)/\omega_{TO,j}^2]^{1/2}$, where $\omega_{LO,j}$ and $\omega_{TO,j}$ are the LO and TO frequencies of jth phonon mode, to estimate the size of the LO-TO splitting. This LO-TO splitting is much larger in r-TiO$_2$ than in r-SnO$_2$, especially for the E^1_u and A$_{2u}$ modes, with $S_j = 1.53$ and 5.01, respectively (Table V), indicating stronger interaction between the Coulomb electric field and the phonons. This effect can be further identified from the Born effective charges. Due to the crystal symmetry of rutile, the Born effective charge tensor has three independent components Z_{xx}^*, Z_{xy}^*, and Z_{zz}^* (x, y, and z represent Cartesian directions). The calculated Born effective charges of r-TiO$_2$ are larger than those of r-SnO$_2$, especially for Z_{zz}^* and Z_{xx}^* (Table V). This is the same for the anatase structure. a-TiO$_2$ has larger Born effective charges than that of a-SnO$_2$. Since

TABLE III. Calculated high frequency and static dielectric constants ε^∞ and ε^0 together with the experimental values. The ∥ and ⊥ represent the x-y plane and z-direction, respectively.

| | ε^∞ | | | | ε^0 | | | |
| | This work | | Expt. | | This work | | Expt. | |
	⊥	∥	⊥	∥	⊥	∥	⊥	∥
r-SnO$_2$	3.7	3.9	3.8[a]	4.2[a]	12	7.0	14[a]	9.6[a]
r-TiO$_2$	5.8	7.0	6.8[b]	8.4[b]	70	159	86[c]	170[c]
a-SnO$_2$	3.2	3.5			4.1	4.9		
a-TiO$_2$	5.5	5.3	5.8[d]	5.4[d]	43	13	45[d]	23[d]

[a]Reference 26.
[b]Reference 27.
[c]Reference 28.
[d]Reference 29.

TABLE IV. The calculated infrared-active phonon frequencies of SnO_2 and TiO_2 at Γ point using finite displacement method with non-analytical correction together with the experimental values. The frequencies are in units of meV. $S_j = [(\omega_{LO,j}^2 - \omega_{TO,j}^2)/\omega_{TO,j}^2]^{1/2}$, where $\omega_{LO,j}$ and $\omega_{TO,j}$ are the LO and TO frequencies of the jth phonon mode (… represent there is no corresponding vibration modes).

	r-SnO$_2$			r-TiO$_2$			a-SnO$_2$		a-TiO$_2$		
	This work	Expt.[a]	S_j	This work	Expt.[b]	S_j	This work	S_j	This work	Expt.[c]	S_j
E_u^1(TO)	32.3	30.2		25.7	23.6		30.6		31.4	32.5	
E_u^1(LO)	34.7	34.3	0.39	47.0	46.3	1.53	36.4	0.57	39.5	45.5	0.77
E_u^2(TO)	36.5	36.4		48.4	48.0		92.5		51.2	54.2	
E_u^2(LO)	50.4	45.1	0.95	57.2	53.4	0.63	93.1	0.09	105	109	1.78
E_u^3(TO)	73.7	76.5		57.3	61.2		…	…	…	…	…
E_u^3(LO)	94.7	95.5	0.81	96.0	104	1.34	…	…	…	…	…
A_{2u}(TO)	59.1	59.2		15.0	21.5		73.7		46.2	45.5	
A_{2u}(LO)	79.7	87.3	0.91	76.8		5.01	92.8	0.78	77.7	93.5	1.35

[a]Reference 32.
[b]References 30 and 33.
[c]Reference 29.

SnO_2 and TiO_2 isostructure polymorphs have the same crystal symmetry, the origin of the different Born effective charges may be explained from the Ti−O and Sn−O bonding based on the idea of bond charge model.[34] The strong ionic Ti−O bonds give rise to large Born effective charges, thereby a large LO-TO splitting. Interestingly, the LO-TO splitting in r-TiO$_2$ is much larger than in a-TiO$_2$ although they have the same chemical compositions. The Born effective charges in a-TiO$_2$ structure along the [100] and [001] directions are listed in Table V. In order to better compare the Born charges of r-TiO$_2$ and a-TiO$_2$, the Born effective charges of r-TiO$_2$ were diagonalized with the axes along [110], [$\bar{1}$10], and [001] directions: Z_{xx}^*(Ti) = 6.20, Z_{yy}^*(Ti) = 5.20, Z_{zz}^* (Ti) = 7.35, Z_{xx}^*(O) = −4.54, Z_{yy}^*(O) = −1.22, Z_{zz}^*(O) = −3.71. The larger Z_{zz}^* (Ti) and Z_{zz}^*(O) in r-TiO$_2$ may be understood as local structure distortion. It has been demonstrated that the Born effective charge in $BaTiO_3$ are strongly dependent on the details of the crystal structure.[35] In the rutile structure of SnO_2 and TiO_2, the cation located in octahedron central with the four of the O atoms in the same plane and the O is surrounded by three cation atoms (i.e., Ti−O−Ti angle is ∼98° and 131°). In anatase structure, however, the octahedrons are distorted with two O atoms upwards and the other two downwards (i.e., O−Ti−O bond angle is ∼102°) and the O is surrounded by three cation atoms (i.e., Ti−O−Ti angle is ∼154°). This

TABLE V. The Born effective charge of SnO_2 and TiO_2 calculated from the derivative of the force on nuclei by a homogeneous effective electric field at the zero atomic displacement. The x, y, z directions along the a, b, and c crystal axis in the conventional cell of rutile and anatase. For rutile structure, only Z_{xx}^* is presented ($Z_{xx}^* = Z_{yy}^*$).

	Rutile				Anatase			
	Sn	O	Ti	O		Sn	O	Ti	O
Z_{xx}^*	4.14	−1.93	5.70	−2.88	Z_{xx}	4.20	−0.90	5.96	−5.12
Z_{xy}^*	0.29	−0.67	1.89	−1.66	Z_{yy}	4.20	−2.86	5.96	−0.75
Z_{zz}^*	4.45	−2.06	7.35	−3.71	Z_{zz}	4.11	−1.82	6.47	−2.70

distortion of the local structure in anatase may result in a decrease of the Born effective charge and hence a smaller LO-TO splitting.

D. Electron-phonon coupling

The large LO-TO splitting has a strong impact on the dielectric function of phonon part. The three E_u modes and one A_{2u} mode exhibit LO-TO splitting corresponding to three response peaks in the [100] direction and one in the [001] direction in the $\varepsilon_1(\omega)$ which is infinite at the frequency ω_{TO} and completely reflection in the LO-TO frequencies range (Fig. 7) in the limit of zero damping parameter. The modeled static dielectric constants ε^0 of the compounds agree well with the experimental values (Table III),[26–29] The large ε^0 in both SnO_2 and TiO_2 demonstrates the importance of taking into the account the electron-phonon coupling, especially ε^0 of r-TiO$_2$ ($\varepsilon_\perp^0 = 70$ and $\varepsilon_\parallel^0 = 159$) which is much larger than that of r-SnO$_2$ ($\varepsilon_\perp^0 = 13$ and $\varepsilon_\parallel^0 = 7.0$) and a-TiO$_2$ ($\varepsilon_\perp^0 = 43$, $\varepsilon_\parallel^0 = 13$ for a-TiO$_2$). This is due to the stronger ionic Ti-O bonds and structure distortion in the r-TiO$_2$.

The strong ionic bonds screen the carries and create polarons. The polarons couple to the electrons and this interaction can be described as a change in the effective masses. By using the Fröhlich electron-phonon coupling model,[36] the polaron effective mass is simulated by $m^p = m^*/(1 + \alpha/6)$, where $\alpha = (2e^4 m^*/2\hbar^3 \omega_{LO})^{1/2} (\varepsilon^{0-1} - \varepsilon^{\infty -1})$ is the Fröhlich constant. Since α is larger in TiO_2 compared to SnO_2, this shows that the polaron effect in TiO_2 is very strong, generating a larger polaron masses ($m_{v_1,\perp}^p / m_{v_1,\perp}^* = 2.89$ and 2.54 for rutile and anatase, respectively; see Table II). In r-SnO$_2$, although the ionic bonding is weaker than r-TiO$_2$, the relatively smaller ω_{LO} and consequently larger Fröhlich constant α give rise to larger polaron mass which is not negligible in studying the electron conductivity. Due to the larger ratio of $\varepsilon_\perp^0/\varepsilon_\perp^\infty$, the transverse hole polaron mass $m_{v_1,\perp}^p$ is also larger than its corresponding longitudinal mass $m_{v_1,\parallel}^p$, although the transverse hole bare mass $m_{v_1,\perp}^*$ is smaller than its corresponding longitudinal mass $m_{v_1,\parallel}^*$.
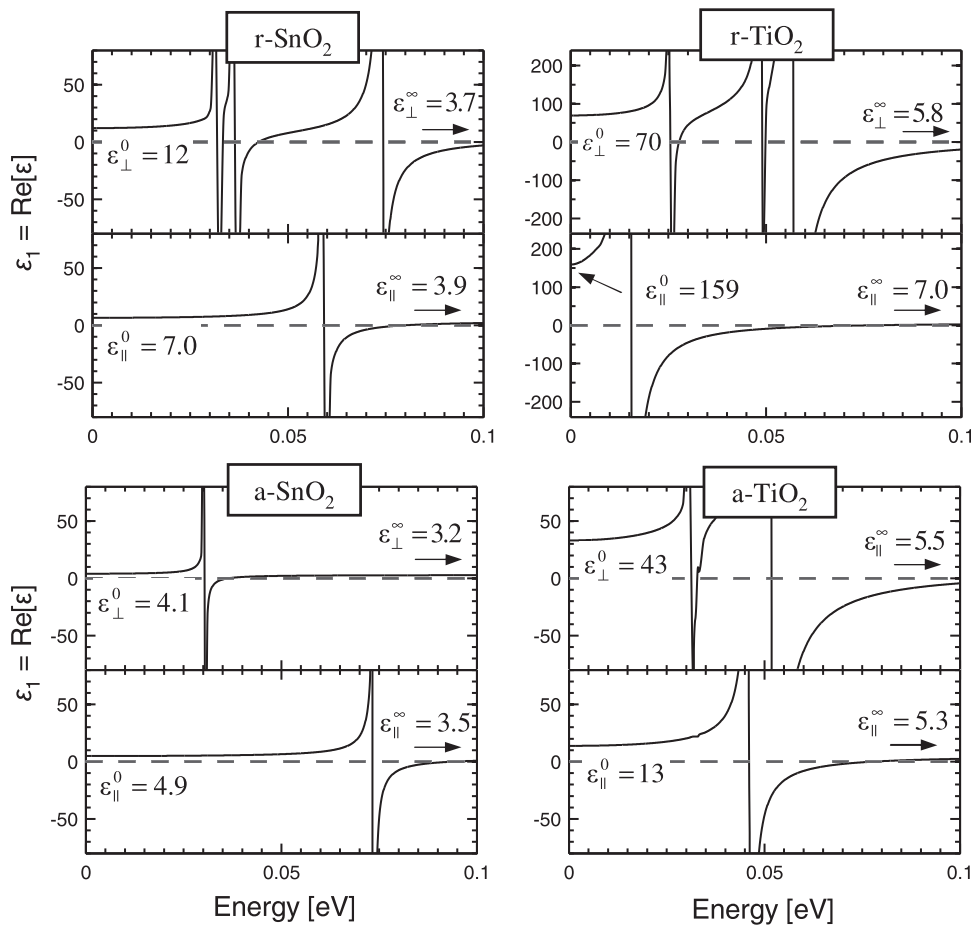
FIG. 7. The phonon parts of real dielectric functions simulated from the Lorentz model and Kramers-Heisenberg formula with multiphonon contributions in the limit of zero damping parameter ($\gamma_j \to 0$). The spectra are divided into transverse and longitudinal components, with the corresponding LO-TO splitting calculated using non-analytical correction.

IV. CONCLUSION

The SnO_2 and TiO_2 (both rutile and anatase) have comparable band-gap energies but different band-edges structures: single and highly dispersive CBs for SnO_2 but flat and energetically close-lying CBs for TiO_2 due to the different cation valence electrons' configuration. The Ti-$3d$ electrons also give rise to the large anisotropy effective electron masses of TiO_2.

The calculated dielectric functions reveal weak optical direct transition in the photon energy region $E_g \leq \hbar\omega \leq E_g + \Delta$ for r-SnO_2, r-TiO_2, and a-SnO_2 (where $\Delta = 0.72, 0.38$, and 0.63 eV for r-SnO_2, r-TiO_2, and a-SnO_2, respectively) due to the symmetry of the wavefunctions of the highest VB and the lowest CB. The main on-set to absorption occurs at $\hbar\omega \approx E_g + \Delta$. In a-$TiO_2$, however, the direct optical transition on-set is at $\hbar\omega \approx 3.9$ eV which is between E_g and the $E_g + \Delta$ corresponding to the transition from uppermost VB to the bottommost CB along $\Gamma-Z$ direction. The flat and energetically close-lying CBs in TiO_2 contribute to a large optical absorption coefficient. TiO_2, both rutile and anatase, have larger LO-TO splitting and ε^0 than SnO_2 due to the strong ionic Ti$-$O bonds.

[1]D. F. Zhang, L. D. Sun, J. L. Yin, and C. H. Yan, Adv. Mater. **15**, 1022 (2003); E. Fortunato, P. Barquinha, and R. Martins, *ibid.* **24**, 2945 (2012).
[2]G. Sberveglieri, Sens. Actuators, B **6**, 239 (1992); S. R. Davis, A. Wilson, and J. D. Wright, IEE Proc.: Circuits Devices Syst. **145**, 379 (1998).
[3]S. A. Campbell, D. C. Gilmore, X. C. Wang, M. T. Hsieh, H. S. Kim, W. L. Gladfelter, and J. Yan, IEEE Trans. Electron Devices **44**, 104 (1997); K. Kim, C. G. Hwang, and J. G. Lee, *ibid.* **45**, 598 (1998).
[4]C. D. Canestraro, M. M. Oliveira, R. Valaski, M. V. S. da Silva, D. G. F. David, I. Pepe, A. F. da Silva, L. S. Roman, and C. Persson, Appl. Surf. Sci. **255**, 1874 (2008); C. D. Canestraro, L. S. Roman, and C. Persson, Thin Solid Films **517**, 6301 (2009).
[5]C. Persson and S. Mirbt, Braz. J. Phys. **36**, 286 (2006); C. Persson and A. Ferreira da Silva, Appl. Phys. Lett. **86**, 231912 (2005).
[6]C. Persson and A. Zunger, Phys. Rev. B **68**, 073205 (2003); F. Thomazi, L. S. Roman, A. F. Silva, and C. Persson, Phys. Status Solidi C **6**, 2740 (2009).
[7]C. L. Dong, C. Persson, L. Vayssieres, A. Augustsson, T. Schmitt, M. Mattesini, R. Ahuja, C. L. Chang, and J. H. Guo, Phys. Rev. B **70**, 195325 (2004).
[8]J. Heyd, G. E. Scuseria, and M. Ernzerhof, J. Chem. Phys. **118**, 8207 (2003); **124**, 219906 (2006).
[9]G. Kresse and D. Joubert, Phys. Rev. B **59**, 1758 (1999); P. E. Blöchl, *ibid.* **50**, 17953 (1994).
[10]A. Togo, F. Oba, and I. Tanaka, Phys. Rev. B **78**, 134106 (2008).
[11]X. Gonze and C. Lee, Phys. Rev. B **55**, 10355 (1997); Y. Wang, J. J. Wang, W. Y. Wang, Z. G. Mei, S. L. Shang, L. Q. Chen, and Z. K. Liu, J. Phys.: Condens. Matter **22**, 202201 (2010).
[12]M. Gajdoš, K. Hummer, G. Kresse, J. Furthmüller, and F. Bechstedt, Phys. Rev. B **73**, 045112 (2006).
[13]H. Kuzmany, *Solid State Spectroscopy: A Introduction* (Springer, Berlin, 2009), p. 117; S. Meneses, J. F. Brun, P. Echegut, and P. Simon, Appl. Spectrosc. **58**, 969 (2004), and the references therein.

[14]O. Madelung, *Semiconductor Basic Data*, 2nd revised ed. (Springer, Berlin, 1996), p. 201.

[15]J. Pascual, J. Camassel, and H. Mathieu, Phys. Rev. B **18**, 5606 (1978).

[16]Y. Tezuka, S. Shin, T. Ishii, T. Ejima, S. Suzuki, and S. Sato, J. Phys. Soc. Jpn. **63**, 347 (1994).

[17]H. Tang, K. Prasad, R. Sanjines, P. E. Schmid, and E. Levy, J. Appl. Phys. **75**, 2042 (1994).

[18]H. Tang, F. Levy, H. Berger, and P. E. Schmid, Phys. Rev. B **52**, 7771 (1995).

[19]G. Sanon, R. Rup, and A. Mansingh, Phys. Status Solidi A **135**, 581 (1993); J. A. Marley and R. C. Dockerty, Phys. Rev. B **140**, A304 (1965).

[20]R. G. Berckenridge and W. R. Hosler, Phys. Rev. **91**, 793 (1953).

[21]M. Stamate, G. Lazar, and I. Lazar, Rom. J. Phys. **53**, 217 (2008).

[22]L. Chiodo, J. M. García-Lastra, A. Iacomino, S. Ossicini, J. Zhao, H. Petek, and A. Rubio, Phys. Rev. B **82**, 045207 (2010).

[23]J. Kang, S. Tsunekawa, and A. Kasuya, Appl. Surf. Sci. **174**, 306 (2001); A. Amtout and R. Leonelli, Phys. Rev. B **51**, 6842 (1995).

[24]Z. Wang, U. Helmersson, and P. O. Käll, Thin Solid Films **405**, 50 (2002).

[25]W. Kang and M. S. Hybertsen, Phys. Rev. B **82**, 085203 (2010), and the references therein.

[26]Collaboration: Authors and editors of the volumes III/17E-17F-41C, "Tin dioxide (SnO_2) optical properties, dielectric constants," in *Springer Materials-The Landolt-Börnstein Database*, edited by O. Madelung, U. Rössler, and M. Schulz (Springer).

[27]T. A. Darvis and K. Vedam, J. Opt. Soc. Am. **58**, 1446 (1968).

[28]P. A. Parker, Phys. Rev. **124**, 1719 (1961).

[29]R. J. Gonzalez, R. Zallen, and H. Berger, Phys. Rev. B **55**, 7014 (1997).

[30]J. G. Traylor, H. G. Smith, R. M. Nicklow, and M. K. Wilkinson, Phys. Rev. B **3**, 3457 (1971).

[31]T. Ohsaka, F. Izumi, and Y. Fujiki, J. Raman Spectrosc. **7**, 321 (1978).

[32]R. S. Katiyar, P. Dawson, M. M. Hargreave, and G. R. Wilkinson, J. Phys. C **4**, 2421 (1971).

[33]D. M. Eagles, J. Phys. Chem. Solids **25**, 1243 (1964).

[34]K. Hübwer, Phys. Status Solidi B **68**, 223 (1975).

[35]P. Ghosez, J. P. Michenaud, and X. Gonze, Phys. Rev. B **58**, 6224 (1998).

[36]M. P. Marder, *Condensed Matter Physics*, 2nd revised ed. (Wiley, New Jersey, 2010), p. 671.